

International Conference on Space Optics—ICSO 2014

La Caleta, Tenerife, Canary Islands

7–10 October 2014

Edited by Zoran Sodnik, Bruno Cugny, and Nikos Karafolas



PILOT: optical performance and end-to-end characterisation

Y. Longval

R. Misawa

P. Ade

Y. André

et al.



International Conference on Space Optics — ICSO 2014, edited by Zoran Sodnik, Nikos Karafolas,
Bruno Cugny, Proc. of SPIE Vol. 10563, 105635X · © 2014 ESA and CNES
CCC code: 0277-786X/17/\$18 · doi: 10.1117/12.2304278

PILOT: OPTICAL PERFORMANCE AND END-TO-END CHARACTERISATION

Y. Longval¹, R. Misawa², P. Ade⁵, Y. André⁷, P. deBernardis⁴, F. Bousquet⁷, M. Bouzit¹, V. Buttice¹, M. Charra¹, B. Crane¹, J.P. Dubois¹, C. Engel², M. Griffin⁵, P. Hargrave⁵, B. Leriche¹, S. Maestre², C. Marty², W. Marty², S. Masi⁴, B. Mot², J. Narbonne², F. Pajot¹, G. Pisano⁵, N. Ponthieu⁶, I. Ristorcelli², L. Rodriguez³, G. Roudil¹, O. Simonella⁷, M. Salatino⁴, G. Savini⁵, C. Tucker⁵, J-P Bernard²

¹ Institut d'Astrophysique Spatiale (IAS), Bât 121, Université Paris XI, Orsay, France;

² Institut de Recherche en Astrophysique et Planetologie (IRAP), 9 Av du Colonel Roche, BP 4346, 31028 Toulouse cedex 4, France;

³ CEA/Saclay, 91191 Gif-sur-Yvette Cedex, France;

⁴ Università degli studi di Roma "La Sapienza", Dipartimento di Fisica, P.le A. Moro, 2, 00185, Roma, Italia;

⁵ Department of Physics and Astrophysics, PO BOX 913, Cardiff University, 5 the Parade, Cardiff, UK;

⁶ Grenoble University, Grenoble, France;

⁷ Centre National des Etudes Spatiales, DCT/BL/NB, 18 Av. E. Belin, 31401 Toulouse, France.

I. INTRODUCTION

PILOT (Polarized Instrument for the Long-wavelength Observations of the Tenuous ISM), is a balloon-borne astronomy experiment dedicated to study the polarization of dust emission from the diffuse ISM in our Galaxy [1]. The observations of PILOT have two major scientific objectives. Firstly, they will allow us to constrain the large-scale geometry of the magnetic field in our Galaxy and to study in details the alignment properties of dust grains with respect to the magnetic field. In this domain, the measurements of PILOT will complement those of the Planck satellite at longer wavelengths. In particular, they will bring information at a better angular resolution, which is critical in crowded regions such as the Galactic plane. They will allow us to better understand how the magnetic field is shaping the ISM material on large scale in molecular clouds, and the role it plays in the gravitational collapse leading to star formation. Secondly, the PILOT observations will allow us to measure for the first time the polarized dust emission towards the most diffuse regions of the sky, where the measurements are the most easily interpreted in terms of the physics of dust. In this particular domain, PILOT will play a role for future CMB missions similar to that played by the Archeops experiment for Planck. The results of PILOT will allow us to gain knowledge about the magnetic properties of dust grains and about the structure of the magnetic field in the diffuse ISM that is necessary to a precise foreground subtraction in future polarized CMB measurements. The PILOT measurements, combined with those of Planck at longer wavelengths, will therefore allow us to further constrain the dust models. The outcome of such studies will likely impact the instrumental and technical choices for the future space missions dedicated to CMB polarization.

The PILOT instrument will allow observations in two photometric channels at wavelengths 240 μm and 550 μm , with an angular resolution of a few arcminutes. We will make use of large format bolometer arrays, developed for the PACS instrument on board the Herschel satellite. With 1024 detectors per photometric channel and photometric band optimized for the measurement of dust emission, PILOT is likely to become the most sensitive experiment for this type of measurements. The PILOT experiment will take advantage of the large gain in sensitivity allowed by the use of large format, filled bolometer arrays at frequencies more favorable to the detection of dust emission.

This paper presents the optical design, optical characterization and its performance. We begin with a presentation of the instrument and the optical system and then we summarise the main optical tests performed. In section III, we present preliminary end-to-end test results.

II. THE OPTICAL SYSTEM

PILOT is a balloon-borne experiment designed to fly at a ceiling altitude of around 40 km (4 hPa pressure) in the stratosphere. A generic CNES stabilized gondola, with azimuthal coarse pointing control, will carry the experiment, as shown in Fig. 1.

Mapping of the sky will be accomplished by rotating the gondola over a large azimuth range ($\pm 30^\circ$) at a constant elevation, in order to reduce the residual atmospheric contribution. The pointing elevation of the payload can range from 20° to 60° . The fine attitude of the instrument and the effective pointing directions will be reconstructed a posteriori, using the signal from a fast, large format CCD stellar sensor co-aligned with the instrument optical axis. The fastest (1.2°/s) rotation speed for the azimuth scanning is a compromise between, on the one hand, the need to cover a large amplitude and to reduce the instrument drifts, and, on the other hand, the need to distinguish point

sources detection from parasitic "spikes", and respect both the detectors and the stellar sensor response times. The total gondola mass will be of the order of 1100 kg.

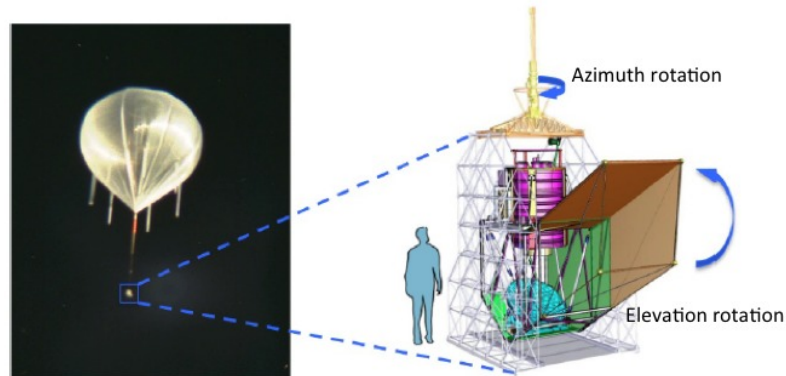


Figure 1. Schematic view of the PILOT gondola. The cryostat (cylinder on top) and the primary mirror are attached to the pointed load, which can rotate around its elevation axis. Motion around the flight chain will be carried by the azimuth swivel.

A. Optical layout

The optics of PILOT have been designed in order to provide a large instantaneous field of view of about $0.8^\circ \times 1^\circ$, an equivalent focal distance of 1800 mm and a F/2.5 numerical aperture. Its angular resolution is better than 3.5 arcminutes at 500 microns. Its optical layout is shown on Fig.2. It combines a large primary mirror (M1) and a cooled Photometer at 3K including the cold optics. It consists of three optical subsystems: telescope, re-imager and polarimeter [2].

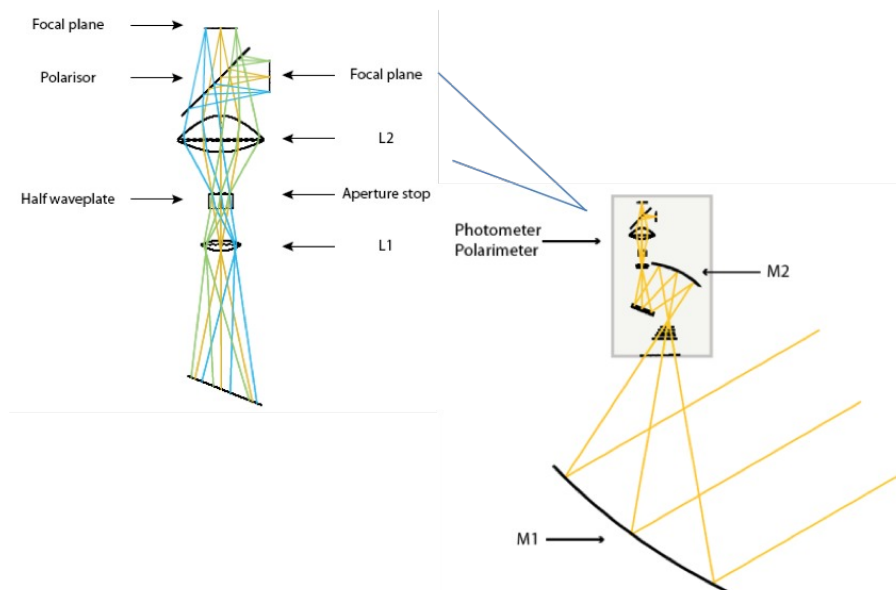


Figure 2. Optic Layout of PILOT.

The telescope is an off-axis Gregorian telescope. It is composed mainly of an off-axis paraboloid mirror M1 with a large diameter and an off-axis ellipsoid mirror M2, in order to avoid central obscuration. Both mirrors are made of Aluminum. Their off-axis distances, tilt angles and focal distances are combined to satisfy the Mizugushi-Dragnone condition [3], and form an equivalent on-axis parabola to minimize instrumental polarization effects.

The reimaging optics consists of two polypropylene lenses forming a telecentric objective. The first lens L1 is at the telescope focal plane, it images the primary mirror onto the cold Aperture stop; the second lens L2 images the telescope focal plane onto the detectors.

A flat mirror M3 is used to fold the beam to reduce the Phtometer volume.

The polarimeter consists of a rotating Half WavePlate (HWP) and a fixed polarizer. The HWP is placed near the cold stop and is motorized in rotation to change the polarization direction of incoming fields.

The half wave-plate is made of sapphire with five thin plates designed for the dual spectral bands 240 μm and 550 μm [4].

Concerning the rejection of the straylight (coming from the ground, balloon, and the emission and diffraction of warm objects), there are two stops in the photometer: one is a Field Stop at the telescope focal plane, with a similar form of the detector array plane; and the other is an cold Aperture Stop, located between the two lenses.

All optical elements except the primary mirror constitute the cold optics, and are located in a 3K cryostat.

This optical configuration is optimized to provide a diffraction limited image quality all over the large focal plane and to minimize straylight.

B. Subsystem Characterization

The primary mirror is an off-axis parabola with a diameter of 980 mm. Its optical parameters were measured using a 3D machine and verified by optical measurement, including surface curvature, conic constant, off-axis distance. Its characterization was performed on a dedicated optical bench, used for ODIN telescope; the details are described in [5].

The secondary mirror is an off-axis elliptical mirror with 200 mm diameter; it plays a critical role in combining the M1 into the Photometer by its two focus. We need to check and align M2 and M3 by classical optical means at visible wavelength. M2 is made of aluminum and manufactured by numerical diamond machining. Its surface is of optical quality with a surface accuracy of 0.3 μm in P-V, and the roughness of 10 nm in RMS.

Its optical surface parameters were measured with a 3D machine and checked with a Point Diffraction Interferometer. Fig.3 shows the optical test bench. It composed of a He-Ne laser, a microscope objective, a pinhole, the mirror M2 under tested and a reflective ball. The pinhole and the ball are placed at the ellipsoid mirror M2's two focus position respectively. A beam splitter, placed between M2 and the ball, extracts a part of the beam and send to the PDI interferometer. Fig.4 the interference pictures obtained. The middle picture shows the almost perfect interference picture when the secondary focus was at the right position; and the left and the right pictures show the ones for defocused positions.

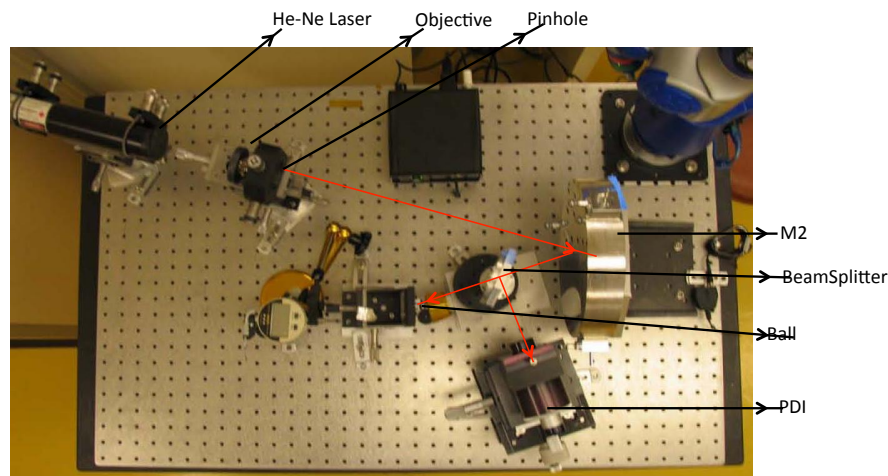


Figure 3. Picture of the optical test bench.



Figure 4. The obtained interference pictures.

The two refractive lenses, L1 and L2, are made of polymer. Some polymers present non-homogeneous characteristics depending on their manufacturing process.

The knowledge of the optical properties of the material is of great importance to the instrument polarization performance. We developed an optical bench to characterizing the polarization effects of materials and tested three different polymer materials: polypropylene, polyethylene HDPE, and UHMW. The results showed that the

polypropylene samples (three samples cut from three orthogonal axes) presented non-obvious polarization effects. But this was not the case for other two materials. So we choose polypropylene for the lenses and windows material.

We measured the polypropylene refractive index, its transmission and thermo-elastic parameter both at room temperature and at cryonic temperature.

The obtained refractive index values are 1.500 ± 0.004 at room temperature, and 1.524 ± 0.006 at 4K.

The transmission was measured with 2 mm and 10 mm thickness samples, and the obtained values are 0.865 ± 0.004 and 0.649 ± 0.002 respectively.

The thermal expansion factor was measured with 2 mm thickness sample at room temperature and at 77K; we obtained the total contraction is 1.14%, which is concordant to the value of 1.15% at 80K described in [6]. So we take 1.25% for 4K as in [6].

The lenses were manufactured using a 3D cutting tool and their surface parameters were obtained by fitting the data measured using a 3D machine.

All the realistic optical and thermo-elastic parameters of the optical elements are taken into account in our optical simulation, thermo-elastic analysis and alignment procedure.

C. Optical Alignment

The requirement on the overall optical quality of the PILOT instrument translates into the alignment between the primary mirror and the photometer and leads to a required accuracy of about $300 \mu\text{m}$ for the focus relative positions, and a maximum mismatch of 0.06° for their optical axes orientations. This requirement must be satisfied at all time during the observations at ceiling altitude, while the elevation of the pointed load is changed and the temperature of the structure evolves producing thermo-elastic deformation. This is actually one of the most stringent requirements for the experiment.

Fulfilling this requirement has implied a series of actions: First, precise characterizations of the mechanical and optical properties of the primary mirror and of the photometer have been carried out separately. The mirror characterization was performed using a submillimeter test bench. The photometer optical characteristics were determined using ZEMAX simulations, together with optical and 3D measurements. Second, specific tools and an efficient procedure have been developed to align the two subsystems, both for ground test and before flight. To perform this alignment, the primary mirror is mounted on a hexapod, which allows six degrees of freedom for the adjustment while maintaining the stiffness of the system. A numerical model of this mechanism allows a fast convergence of the optical alignment. The relative position of the two subsystems is checked by measuring, using a laser tracker system, a series of optical reference balls associated with the mirror and the photometer. Third, despite the fact that the whole structure connecting the photometer and M1, and the M1 mirror itself are made of the same material (aluminum), which limits differential dilatation, the optical system is off-axis and no perfect compensation of thermo-elastic effects is possible. In order to control the optical alignment during flight, a thermal model of the instrument has been developed. Before launch, the use of this model, knowing the temperature during flight, will allow us to correct for the expected displacement, compensating to first order the effect of the thermal expansion of the mechanical structure expected at ceiling altitude. Fourth, deformations of the holding structure due to gravity at the various elevations have been modeled using a finite element analysis based on Nastran. These deformations are expected to be somewhat lower than thermal deformations. They have also been measured during tests.

D. Photometer Spectral characterization

The fine knowledge of the instrument spectral response is important for the determination of both the effective wavelength and the polarization parameters of the measurement. Spectral band mismatch between the two polarized focal planes can induce systematic errors in the polarization properties determination. Indeed, we use two sets of bandpass filters at $240 \mu\text{m}$ for the transmission channel and for the reflection channel respectively. Therefore a precise spectral calibration of the two focal plane arrays is required.

The optical bench developed for the spectral test and calibration is based on a Martin-Puplett type Fourier transform spectrometer (FTS). This method was successfully used for the Planck/HFI spectral calibration [7]. This bench (Fig. 5) allowed characterizing the overall spectral response of the instrument.

The characterization was performed for two polarized beams coming from the FTS and for all angular positions of the half-wave plate. Fig.5. shows the measured spectral response for 3 HWP positions (positions 1, 3 and 5) on one of the arrays [8].

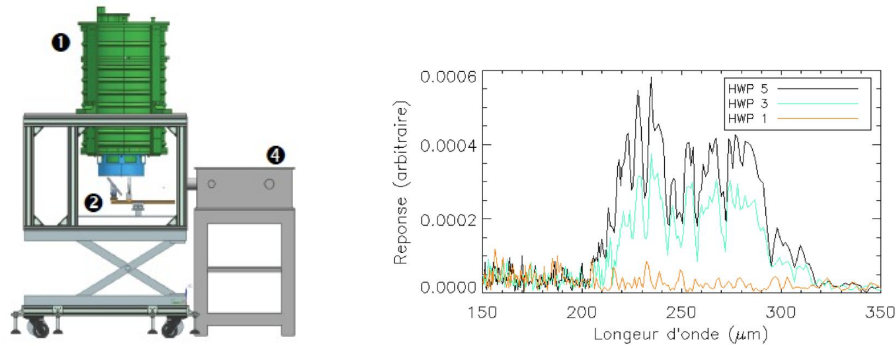


Figure 5. Left: test optical bench. Right: Spectral response for HWP at 1, 3 and 5 positions for one of the arrays.

III. GROUND TEST PERFORMANCES

The aim of the PILOT ground tests was to validate the instrument behaviour and to optimize its performance. These tests were performed in a clean room at the CNES facilities in Toulouse, France [9]. Since the background falling on the detectors is much stronger in the ground configuration than at ceiling altitude, and because the detectors are optimised for a moderate background, of the order of 5 pW/pixel, we inserted an additional filter in the filter stack, which attenuates the radiation entering the photometer by a factor of 20 at 240 μm wavelength. The spectral transmission of the attenuator was determined according to the predictions of a photometric model of the instrument, taking into account external and internal sources of emission, as well as the transmission of the various optical filters, as measured at the subsystem level. We measured the attenuator spectral transmission by FTS and obtained the results as expected. Thanks to the attenuator, the power received by the detector is adequate during the ground tests.

For these tests, the PILOT instrument was aligned with the IRAP submillimeter bench (see the experimental setup in Fig. 6.) The optical bench is composed of a high intensity lamp (Mercury plasma lamp) at the focus of a Newtonian telescope with a focal length of 5340 mm, delivering a 1 m diameter collimated beam, and acting as a point source at infinite distance. A rotating chopper modulates the source. The source is mounted on a motorized 2D moving plate at the collimator focal plane, so that the parallel beam can scan the instrument focal plane over a limited range, without moving the telescope. For each source central position, the collimated beam direction was measured and referenced with respect to the instrument using theodolites.

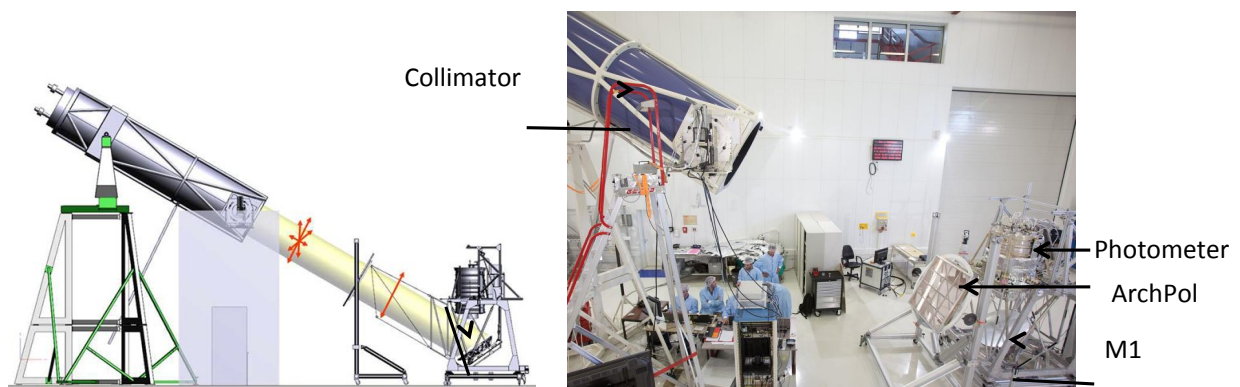


Figure 6 Optical bench for PILOT end-to-end tests.

A. PSF characterization

At 240 μm , the Point Spread Function (PSF) is not Nyquist-sampled, so we used a microscan technique to obtain an over-resolved PSF with higher signal to noise ratio. The microscanning consists in a sub-pixel scan of the point source on the focal plane, with a step of 1/10th pixel. We fitted every image with 2D Gaussian function and we added them up, so as to obtain an experimental PSF that can be compared with the simulated PSFs.

An example of the observed PILOT PSF images is represented in Fig. 7. It shows the PSF images obtained from a microscanning around the pixel (3, 7) of array 6 and array 4, and the comparison between the observed and modeled PSF.

The left and right parts of the figure show the Transmission and Reflection detector arrays respectively. We see PSF images are on the transmission array #6 and the reflection array #4 and notice good symmetry between the

transmission and the reflection detector arrays.

Fig. 7 (a) presents the obtained PSF images during the tests and Fig. 7 (b) presents the PSF images obtained by simulation taking into account the realistic collimator properties. The intensity is normalized and in log scale. The cross patterns around the PSF in low intensity are on all PSF images. They are due to the diffraction of the four struts structure; which support the secondary mirror of the collimator.

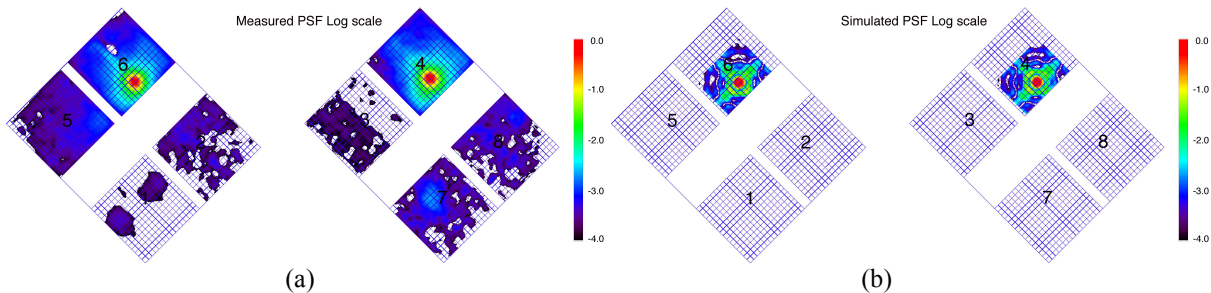


Figure 7. PSF Images on the focal plane. (a): Measured PSF images around a pixel on array #6 and array #4. (b): The corresponding PSF images obtained by simulation taking into account the collimator property.

Fig. 8 shows the obtained and modeled PSF images around the pixel (3, 7) of array #6, and the comparison between the observed and modeled PSF along horizontal and vertical cuts. The observed PSF shows reasonably good agreement with the modeled PSF. The simulations include the realistic source hole dimension and the collimator internal structure, but are computed at a single wavelength. For a better comparison, we will compute the equivalent PSF corresponding to the spectral band transmission of the measurements.

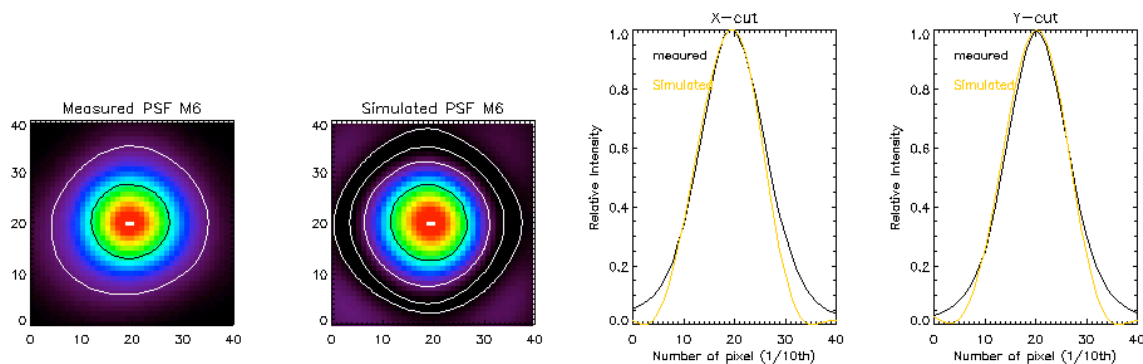


Figure 8. Left: The measured and modeled PSF Images. The intensity is normalized and the dimension of the images is 4*4 pixels. The measured one is obtained from a microscanning pattern around pixel (3, 7) of array #6., the contour levels are at 1.0, 0.5, 0.1, 0.01, and 0.001. Right: profiles along a horizontal and vertical cut. The measured and modeled PSF cuts shown in black and orange respectively.

B. Defocus

In order to determine the best optical alignment of M1 with respect to the photometer, we have performed a series of defocusing along three orthogonal axes, around the best theoretical focus provided by the Zemax model.

The Z defocusing direction corresponds to the optical axis of the photometer while X and Y are orthogonal to it. To estimate the impact of defocusing on the optical performance, all three axis of the focal plane have been explored with the collimator within typically ± 0.8 mm for X, Y axis, and ± 1.6 mm for Z axis. Then the source PSF was fitted in the obtained images, in order to measure the changes in the Full Width of Half Maximum (FWHM) and encircled energy as a function of defocusing distance. The best focus position was determined as the position of minimum FWHM.

Fig. 9 shows an example of the FWHM variation of the PSF at a given position of the focal plane; the defocus offset distance measured from the initial position. The defocus effect in Z-axis is more important than those in X and Y-axis. The variation of FWHM in function of Z defocus is close to a parabolic function; it allowed us to determine the best alignment position.

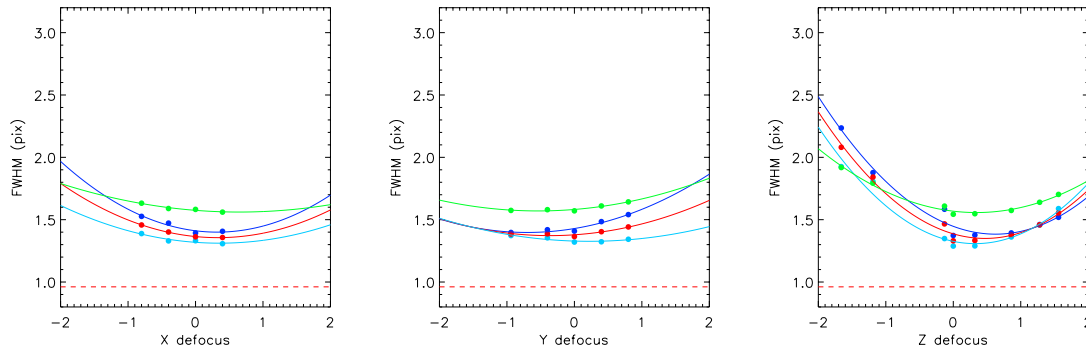


Figure 9. Measured FWHM of the collimator source, as a function of the defocus distance along the X (left), Y (center) and Z (right) on PILOT array #2. FWHM values are in array pixel units, and the defocus is in mm. The horizontal dashed lines show the diffraction limit of the instrument. Blue lines show the FWHM along the X-axis and Cyan lines show the FWHM along the Y-axis. The red lines show the average FWHM over the X and Y-axis and green lines show the FWHM values derived from a circular profile of the PSF.

C. Polarisation

In order to characterize the polarization performance of the instrument, we have used a large (1x1m) polarizer, developed originally for the Archeops balloon-born experiment, hereafter referred to as ArchPol. The ArchPol polarizer is composed of an array of 3x3 frames hosting a large number of metal wires (50 μm thickness, 100 μm separation) and was initially optimized for millimeter wavelengths. The polarizer is inserted in the beam of the collimator as shown in Fig. 4, and can be rotated, in order to produce a polarized source with any polarization direction. Assuming that polarization cross talk of the PILOT instrument is negligible, the polarizer was shown to provide a source polarization fraction higher than 73% in the PILOT 240 μm band. The wire direction of each frame constituting the polarizer was measured with theodolites and laser-tracker. The median wire direction was measured with respect to the polarizer mechanical structure with an accuracy of about 2.4 arcminutes. A series of optical reference balls associated with the polarizer structure allow us to measure its orientation with an accuracy of 1.4 arcminutes. Globally, the direction of linear polarization is known to an accuracy of about 2.4 arcminutes, with respect to the instrument.

Optical calculations show that the direction of an incident linear polarization can be slightly rotated through the optics, as it propagates from the primary mirror to the detector [10], [11]. This rotation angle varies across the focal plane, and, according to calculations, can reach a few degrees. This rotation must be measured precisely and taken into account during astronomical data processing. To characterize this rotation, the whole focal plane has been scanned with the polarizer set at different polarization directions, in order to measure the polarization distortion. For each position, the direction of the polarizer has been measured as described above. We used the polarizer at angles $45.19 \pm 0.30^\circ$ and $-44.81 \pm 0.30^\circ$ and moved the polarized collimator point source over 25 (5x5) pixels of each array. At each position, we rotated the HWP over its full angular range (8 positions). The data is averaged for each PSF position and the PSF flux as a function of HWP position in order to derive polarization parameters. Fig. 10. shows the distribution of the polarization angles over the focal plane. It can be seen that the polarization direction is recovered with the right angle. The actual average recovered values are 45.19° and -44.81° . We noticed the presence of a systematic rotation across the focal plane with an amplitude of about 3° , which is distributed mostly along the cross elevation axis, as expected from the symmetry of the optical system.

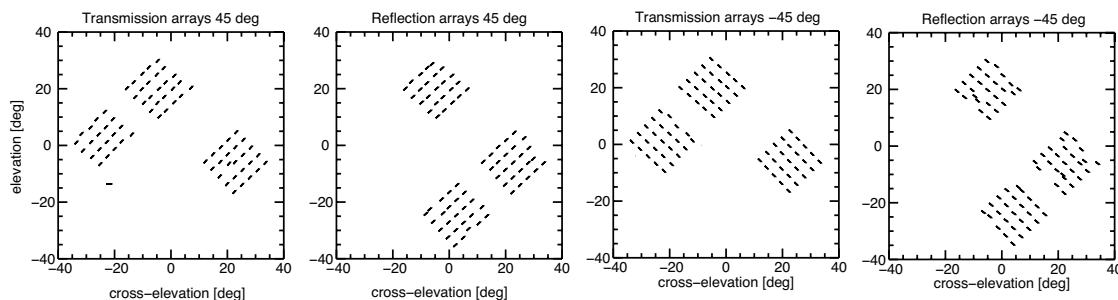


Figure 10. Map of the recovered polarization angles for point sources displaced over 5x5 pixels of each array on the PILOT focal plane. The two left panels show the recovered orientation for the Transmission and Reflexion arrays for an incident polarization angle of 45.19° . The two right panels show the recovered orientation for the Transmission and Reflexion arrays for an incident polarization angle of -44.81° .

IV. CONCLUSION

We have presented the PILOT instrument optical concept, optical tests and its optical achievements.

We have performed a series of ground end-to-end tests of the PILOT experiment, using a collimated source and a large diameter polarizer. We used this system to control the optical performances of the instrument. We measured the width of the PSF of the instrument as a function of defocusing of the primary mirror and found the optimum defocus. The analysis of the PSF shape shows that the optical system is in agreement with expectation from our modeling. Results in polarization indicate that the large-scale polarizer used has 73% polarization efficiency at 240 μm . We tested the performances of the Half-Wave Plate internal to the PILOT photometer and found no evidence of any deviation from perfection. We measured the focal plane distribution of polarization directions for a given direction of the point source polarization and evidenced small rotation through the optical system. These tests demonstrated that the optics of the PILOT system meets the requirements. The data obtained during those tests will be critical to analyze the first scientific data that will be obtained during the first flight of the instrument, scheduled in 2015.

REFERENCES

- [1] Bernard, J.P., Ade, P., de Bernardis, P., Bouzit, M., Engel, C., Giard, M., Griffin, M., Hargrave, P., Laurens, A., Leriche, B., Leroy, C., Longval, Y., Marty, C., Madden, S., Maffei, B., Masi, S., Meny, C., Miville-Deschenes, M.A., Narbonne, J., Nati, L., Pajot, F., Pisano, G., Pointecouteau, E., Ponthieu, N., Ristorcelli, I., Rodriguez, L., Roudil, G., Salatino, M., Savini, G., Torre, G., Tucker, C. "Pilot: measuring polarization in the interstellar medium". In *18th ESA Symposium on European Rocket and Balloon Programmes and Related Research*, 2007.
- [2] C. Engel, Y. Longval · I. Ristorcelli · J. - Ph. Bernard et al, "Optical Design of the PILOT balloon borne experiment: performances and tolerances", unpublished
- [3] C. Dragone, "A first-order treatment of aberrations in Cassegrainian and Gregorian antennas. IEEE Trans. Antennas", Propag. 30, pp. 331–339, 1982.
- [4] G. Pisano, G. Savini, P. Ade, V. Haynes, and W. Gear, "Achromatic half-wave plate for submillimeter instruments in cosmic microwave background astronomy: experimental characterization," Appl. Opt. **45**, pp. 6982-6989, 2006.
- [5] C. Engel, I. Ristorcelli, J.-P., Bernard, Longval, Y., Marty, C., Mot, B., Otrio, G., and Roudil, G., "Characterization and performances of the primary mirror of the PILOT balloon-borne experiment," Experimental Astronomy 36, pp. 21–57, Aug. 2013.
- [6] J. W. Lamb, «Miscellaneous data on materials for millimetre and submillimetre optics,» *International Journal of Infrared and Millimeter Waves*, pp. 1997-2034, 1996.
- [7] F. Pajot et al. "Planck pre-launch status: HFI ground calibration". A&A 520, A10, 2010.
- [8] V. Buttice, "The PILOT camera characterization and spectral calibration", PhD. Thesis, Université Paris Sud, 2013. <http://tel.archives-ouvertes.fr/tel-01023005>
- [9] V. Buttice, et al. "The PILOT experiment for the measurement of interstellar dust polarization: The camera ground calibration", Proc. SPIE, Vol. 8452, 84520U-1-0U-6, 2012
- [9] R. Misawa, J-Ph. Bernard, and al. "PILOT: a balloon-borne experiment to measure the polarized FIR emission of dust grains in the interstellar medium", Proc. SPIE [9153-53], 2014.
- [10] Engel, C. "Optimisation des Performances du Système Optique et Estimation de la Polarisation Instrumentale de l'expérience Embarquée sous Ballon Stratosphérique Pilot", Ph.D. thesis, Université Toulouse III—Paul Sabatier (2012), <http://tel.archives-ouvertes.fr/tel-00821057>
- [11] C. Engel, J.-P. Bernard, G. Otrio, Y. Longval, C. Marty et I. Ristorcelli, «Instrumental polarization modelling for the PILOT submm experiment» *Experimental Astronomy*, unpublished, 2014.